Delamination of a strong film from a ductile substrate during indentation unloading

Abdul-Baqi, A.; van der Giessen, E.

Published in:
Journal of Materials Research

DOI:
10.1016/S0040-6090(00)01344-4

Publication date:
2001

Delamination of a strong film from a ductile substrate during indentation unloading

A. Abdul-Baqi and E. Van der Giessen
Delft University of Technology, Koiter Institute Delft, Mekelweg 2, 2628 CD Delft, The Netherlands

(Received 23 October 2000; accepted 23 February 2001)

In this work, a finite element method was performed to simulate the spherical indentation of a ductile substrate coated by a strong thin film. Our objective was to study indentation-induced delamination of the film from the substrate. The film was assumed to be linear elastic, the substrate was elastic–perfectly plastic, and the indenter was rigid. The interface was modeled by means of a cohesive surface. The constitutive law of the cohesive surface included a coupled description of normal and tagential failure. Cracking of the coating itself was not included. During loading, it was found that delamination occurs in a tangential mode rather than a normal one and was initiated at two to three times the contact radius. Normal delamination occurred during the unloading stage, where a circular part of the coating, directly under the contact area was lifted off from the substrate. Normal delamination was imprinted on the load versus displacement curve as a hump. There was critical value of the interfacial strength above which delamination was prevented for a given material system and a given indentation depth. The energy consumption by the delamination process was calculated and separated from the part dissipated by the substrate. The effect of residual stress in the film and waviness of the interface on delamination was discussed.

I. INTRODUCTION

Industrial application of thin hard-film-coated systems continuously progresses. Coatings are commonly used to enhance reliability, such as chemical resistance, wear resistance, corrosion resistance, and thermal barriers. Adhesion between the film and the substrate determines, to a great deal, the durability of that system. The enhancement gained by the coating may be accompanied by the risk of poor adhesion between the coating and the substrate. Failure of the interface between the coating and the substrate may lead to premature failure of otherwise long lasting systems. Indentation is one of the traditional methods to quantify the mechanical properties of materials, and during the last decades it has also been advocated as a tool to characterize the properties of thin films or coatings. At the same time, for example for hard wear-resistant coatings, indentation can be viewed as an elementary step of concentrated loading. For these reasons, many experimental as well as theoretical studies have been devoted to indentation of coated systems during recent years.

Interfacial delamination is commonly observed in indentation experiments to be accompanied by other failure phenomena, such as coating cracking and subsequent spalling.[1,2] The corresponding load versus displacement curves show a reduction in the stiffness or even a sudden discontinuity which is usually attributed to the coating cracking. Delamination without any accompanying through-thickness cracks has been observed by Li and Bhushan[2] in their nanoindentation experiments on single and multilayer coatings. There is no evidence in the literature, to the authors' knowledge, whether delamination can give rise to any characteristic fingerprint on the load versus displacement curve.

Bagchi and Evans[3] have reviewed the mechanics of thin film decohesion motivated by residual stress. The emphasis in their work is on the role of the interface debond energy and the methods of its quantitative measurement. They argue that most thin film adhesion tests do not measure the interface debond energy because the strain energy release rate cannot be deconvoluted from the work done by the external load. Viable procedures to extract the interfacial energy from indentation experiments will depend strongly on the precise mechanisms involved. The relative contribution of each mechanism to the overall observed behavior and failure mode depends on the material properties and loading conditions in a complex manner. In the case of ductile films on a hard substrate, coating delamination is coupled to plastic expansion of the film with the driving force for

delamination being delivered via buckling of the film (see also Ref. 4). On the other hand, coatings on relatively ductile substrates often fail during indentation by radial and in some cases circumferential cracks through the film. The mechanics of delamination in such systems has been analyzed by Drory and Hutchinson[5] for deep indentation with depths that are 2 to 3 orders of magnitude larger than the coating thickness. They have also reviewed briefly the commonly used test methods for evaluating adhesion.

Hainsworth *et al.*[6] have suggested a simple model for estimating the work of interfacial debonding from the maximum indentation depth and the final delamination radius. In this model, the elastic energy of the indented coating is approximated by the elastic energy of a centrally loaded disc. The idea has also been used in cross-sectional indentation by Sánchez *et al.*[7] as a new technique to characterize interfacial adhesion. The proportionality between the delamination area and the film lateral deflection predicted by the model was confirmed by the experimental results.

The objective of the present paper is to offer an improved understanding of indentation-induced delamination and to test the validity of the above-mentioned simple estimates. For this purpose, we perform a numerical simulation of the process of indentation of thin elastic film on a relatively soft substrate with a small spherical indenter. The complete cycle of the indentation process, both loading and unloading, is simulated. The indenter is assumed to be rigid, the film is elastic and strong, and the substrate is elastic–perfectly plastic. The interface is modeled by a cohesive surface, which allows one to study initiation and propagation of delamination during the indentation process. Separate criteria for delamination growth are not needed in this way. The aim of this study is to investigate the possibility and the phenomenology of interfacial delamination with emphasis on the unloading part of the indentation process and the associated normal delamination. The interfacial failure during the loading part has been studied by the authors in a previous work.[8] Delamination was found to occur in a tangential mode driven by the shear stress at the interface. It is initiated at a radial distance which is two or three times the contact radius resulting in a ring-shaped delaminated area and imprinted on the load–displacement curve as a kind.[8] In this paper we will study the characteristics of normal delamination, conditions for the occurrence/suppression this mode of failure, and its fingerprint on the load–displacement curve and provide some quantitative measures about the interfacial strength. The effect of residual stress in the film and waviness of the interface on delamination will also be investigated. It is emphasized that the calculations assume that other failure events, mainly through-thickness coating cracks, do not occur.

II. PROBLEM FORMULATION

The interface between the coating and the substrate is modeled by means of a cohesive surface, where a small displacement jump between the film and substrate is allowed, with normal and tangential components Δ_n and Δ_t, respectively. The interfacial behavior is specified in terms of a constitutive equation for the corresponding traction components T_n and T_t at the same location. The constitutive law we adopt in this study is an elastic one, so that any energy dissipation associated with separation is ignored. Thus, it can be specified through a potential, i.e.,

$$T_\alpha = -\frac{\partial \phi}{\partial \Delta_\alpha} \quad (\alpha = n, t) \quad . \tag{1}$$

The potential reflects the physics of the adhesion between coating and substrate. Here, we use the potential ϕ that was given by Xu and Needleman[9]

$$\phi = \phi_n + \phi_n \exp\left(-\frac{\Delta_n}{\delta_n}\right)\left\{\left[1 - r + \frac{\Delta_n}{\delta_n}\right]\frac{1-q}{r-1} - \left[q + \left(\frac{r-q}{r-1}\right)\frac{\Delta_n}{\delta_n}\right]\exp\left(-\frac{\Delta_t^2}{\delta_t^2}\right)\right\} \quad . \tag{2}$$

with ϕ_n and ϕ_t the normal and tangential works of separation ($q = \phi_t/\phi_n$) and δ_n and δ_t two characteristics lengths. The parameter r governs the coupling between normal and tangential responses. As shown in Fig. 2, both tractions are highly nonlinear functions of separation with a distinct maximum of the normal (tangential) traction of σ_{max} (τ_{max}) which occurs at a separation of $\Delta_n = \delta_n$ ($\Delta_t = \delta_t/\sqrt{2}$). The normal

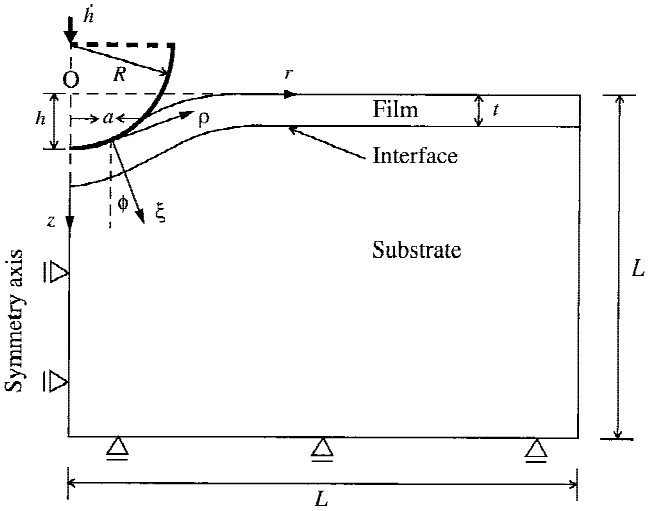

FIG. 1. Geometry of the analyzed problem.

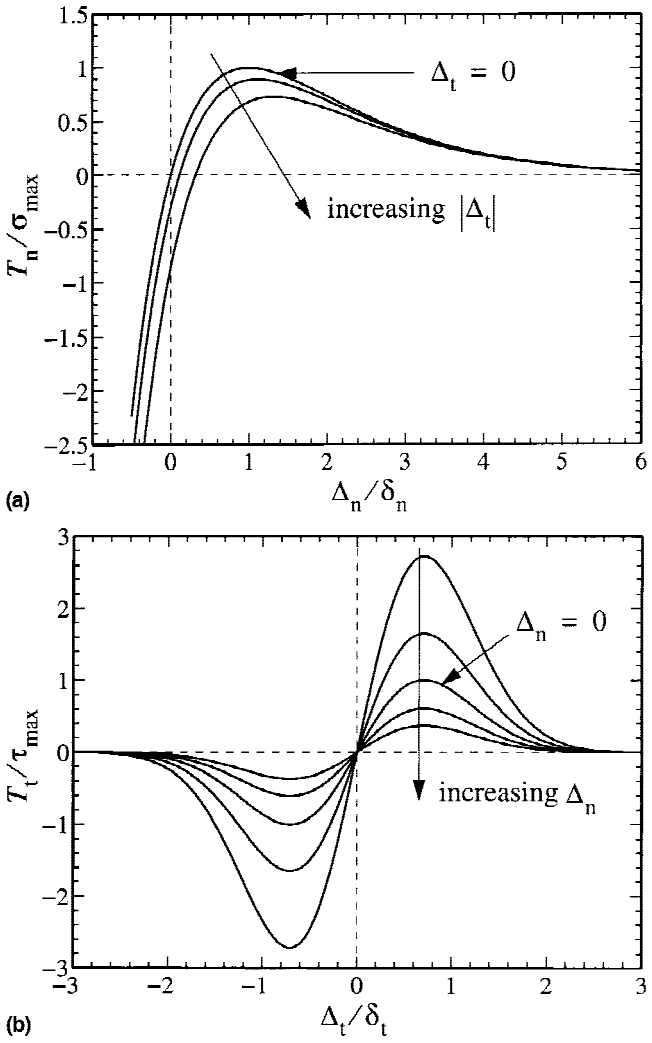

FIG. 2. Normal and tangential responses according to the interfacial potential [Eq. (1)]: (a) normal response $T_n(\Delta_n)$; (b) tangential response $T_t(\Delta_t)$. Both are normalized by their respective peak values σ_{max} and τ_{max}.

(tangential) work of separation, ϕ_n (ϕ_t), can now be expressed in terms of the corresponding strengths σ_{max} (τ_{max}) as

$$\phi_n = \exp(1)\sigma_{max}\delta_n \quad \phi_t = \sqrt{\frac{1}{2}\exp(1)}\tau_{max}\delta_t \quad . \tag{3}$$

Using these along with the definition $q = \phi_t/\phi_n$, we can relate the normal and shear strengths through

$$\sigma_{max} = \frac{1}{q\sqrt{2\exp(1)}}\frac{\delta_t}{\delta_n}\tau_{max} \quad . \tag{4}$$

The coupling parameters r and q are chosen such that the shear peak traction decreases with positive Δ_n and increases with negative Δ_n [Fig. 2(b)]. More details are given in Ref. 8.

The coating is assumed to be a strong, perfectly elastic material with Young's modulus E_c and Poisson's ration ν_c (subscript c for coating).

The substrate is supposed to be a standard isotropic elastoplastic material with plastic flow being controlled by the von Mises stress. For numerical convenience, however, we adopt a rate-sensitive version of this model, expressed by

$$\dot{\eta}_{ij}^{\,p} = \frac{3}{2}\frac{s_{ij}}{\sigma_e}\dot{\epsilon}^p \quad \dot{\epsilon}^p = \dot{\epsilon}_y\left(\frac{\sigma_e}{\sigma_y}\right)^n \quad , \tag{5}$$

for the plastic part of the strain rate, $\dot{\eta}_{ij}^{p} = \dot{\eta}_{ij} = \dot{\eta}_{ij}^{e}$. Here, s_{ij} are the deviator components of the Piola–Kirchhoff stress τ^{ij} and $\dot{\eta}_{ij}$ are the dual Lagrangean strain-rate components. Furthermore, $\sigma_e = \sqrt{(3/2)s_{ij}s^{ij}}$ is the von Mises stress, n is the rate sensitivity exponent, and $\dot{\epsilon}_y$ is a reference strain rate. In the limit of $n \to \infty$, this constitutive model reduces to the rate-independent von Mises plasticity with yield stress σ_y. Values of n on the order of 100 are frequently used for metals (see e.g., Ref. 10), so that the value of σ_e at yield is within a few percent of σ_y for the strain rates that are encountered in our analysis. The elastic part of the strain rate, $\dot{\eta}_{ij}^{e}$, is given in terms of the Jaumann stress rate as

$$\overset{\nabla}{\tau}{}^{ij} = R^{ijkl}\dot{\eta}_{kl}^{e} \quad , \tag{6}$$

with the elastic modulus tensor R^{ijkl} being determined by Young's modulus E_s and Poisson's ration ν_s (subscript s for substrate).

The problem actually solved is illustrated in Fig. 1. The indenter is assumed rigid and to have a spherical tip characterized by its radius R. The film is characterized by its thickness t and is bonded to a half-infinite substrate by an interface specified above. Assuming both coating and substrate to be isotropic, the problem is axisymmetric, with radial coordinate r and axial coordinate z in the indentation direction. The actual calculation is carried out for a substrate of height $L - t$ and radius L, but L is taken large enough so that the solution is independent of L and thus approaches the half-infinite substrate solution.

The analysis is carried out numerically using a finite strain, finite element method. It uses a total Lagrangian formulation in which equilibrium is expressed in terms of the principle of virtual work as

$$\int_v \tau^{ij}\delta\eta_{ij}\,dv + \int_{S_i} T_\alpha\delta\Delta_\alpha\,dS = \int_{\partial v} t^i\delta u_i\,ds \quad . \tag{7}$$

Here, v is the total $L \times L$ region analyzed and ∂v is its boundary, both in the undeformed configuration. With $x^i = (r, z, \theta)$ the coordinates in the undeformed configuration, u_i and t^i are the components of displacement and

traction vector, respectively. The virtual strains $\delta\eta_{ij}$ correspond to the virtual displacement field δu_i via the strain definition,

$$\eta_{ij} = \frac{1}{2}(u_{i,j} + u_{j,i} + u_{k,i}u_{k,j}) \tag{8}$$

where a comma denotes (covariant) differentiation with respect to x^i. The second term in the left-hand side of Eq. (7) is the contribution of the interface, which is here measured in the deformed configuration ($S_i = \{r|z = t\}$). The (true) traction transmitted across the interface has components T_α, while the displacement jump is Δ_α, with α being either the local normal direction ($\alpha = n$) or the tangential direction ($\alpha = t$) in the (r, z)-plane. Here, and in the remainder, the axisymmetry of the problem is exploited, so that $u_\theta = t^\theta = \tau^{i\theta} = \eta_{i\theta} = 0$.

The precise boundary conditions are also illustrated in Fig. 1. The indentation process is performed incrementally with a constant indentation rate $\dot{h}$. Outside the contact area with radius a in the reference configuration, the film surface is traction free,

$$t^r(r, 0) = t^z(r, 0) = 0 \text{ for } a \leqslant r \leqslant L \quad . \tag{9}$$

Inside the contact area we assume perfect sliding conditions. The boundary conditions are specified with respect to a rotated local frame of reference (ρ, ζ, θ) as shown in Fig. 1. In the normal direction, the displacement rate $\dot{u}_\zeta$ is controlled by the motion of the indenter, while in the tangential direction the traction t^ρ is set to zero; i.e.,

$$\dot{u}_\zeta(r, z) = \dot{h}\cos\phi, \quad t^\rho(r, z) = 0 \text{ for } 0 \leqslant r \leqslant a \quad . \tag{10}$$

Numerical experiments using perfect sticking conditions instead have shown that the precise boundary conditions only have a significant effect very close to the contact area and do not alter the results for delamination to be presented later. During the loading part, contact nodes are identified by their spatial location with respect to the indenter; simply, at a certain indentation depth h and displacement increment Δh, the node is considered to be in contact if the vertical distance between the node and the indenter is not greater than Δh. During the unloading part, a node is released from contact on the basis of both its spatial location and the force it exerts on the indenter; if the normal component of the nodal force is smaller than a critical value, and the vertical distance between the node and the indenter is positive, the node is released from contact. The critical value for the nodal force is taken to be 1% of the average current nodal force. It should be noted that using a value 1 order of magnitude smaller did not significantly affect the results. The indentation force F is computed from the tractions in the contact region,

$$F = \int_0^a t^z(r, 0) 2\pi r \, dr \quad . \tag{11}$$

The substrate is simply supported at the bottom, so that the remaining boundary conditions read

$$\begin{aligned} u_z(r, L) &= 0 \quad \text{for } 0 \leqslant r \leqslant L \\ u_r(0, z) &= 0 \quad \text{for } 0 \leqslant z \leqslant L \quad . \end{aligned} \tag{12}$$

However the size L will be chosen large enough that the solution is independent from the precise remote conditions.

III. MODEL PARAMETERS

There are various material parameters that enter the problem, but the main ones are the interfacial normal strength σ_{max}, the coating thickness t, the coating Young's modulus E_c, the maximum indentation depth h_{max}, and the substrate yield strength σ_y. In the results to be presented subsequently we focus mainly on the effect of the interfacial normal strength σ_{max}, keeping the same value of $\sigma_y = 1.0$ GPa (with a reference strain rate of $\dot{\epsilon}_y = 0.1\ s^{-1}$ and $n = 100$). The elastic properties are taken to be $E_c = 500$ GPa, $\nu_c = 0.33$, $E_s = 200$ GPa, and $\nu_s = 0.33$.

For the cohesive surface we have chosen the same values for δ_n and δ_t, namely 0.1 μm. As in the previous study,[8] the coupling parameters r and q are both taken equal to 0.5 which give rise to qualitatively realistic coupling between normal and tangential responses of the interface. The values of σ_{max} that have been investigated vary approximately between 0.5 and 2.0 GPa. These correspond to interfacial energies for normal failure ranging from 150 to 600 J/m^2, which are realistic values for the interface toughnesses of well-adhering deposited films.[11] Note that a constant value of q implies that the shear strength τ_{max} always scales with the normal strength σ_{max} according to Eq. (4).

We have used an indenter of radius $R = 25$ μm and most of the results are for a film thickness $t = 2.5$ μm. Indentation as well as retraction are performed at a constant rate $\dot{h} = \pm 1$ mm/s. The size L of the system analyzed (Fig. 1) is taken to be $50t$. This proved to be large enough that the results are independent of L and therefore identical to those for a coated half-infinite medium. The mesh is an arrangement of 12,000 quadrilateral elements and 12,342 nodes. The elements are built up of four linear strain triangles in a cross arrangement to minimize numerical problems due to plastic incompressibility. To resolve properly the high stress gradients under the indenter and for an accurate detection of the contact nodes, the mesh is made very fine locally near the contact area with an element size of $t/10$.

Consistent with the type of elements in the coating and the substrate, linear two-noded elements are used along the interface. Integration of the cohesive surface contribution in Eq. (7) is carried out using two-point Gauss integration. Failure, or delamination, of the

interface at any location develops when Δ_α exceeds δ_α. A practical definition of when a complete crack has formed is $\Delta_\alpha = 2\delta_\alpha$.[12]

The maximum indentation depth applied in all calculations is $h_{max} \leqslant 2t$. Further indentation can be done but was not considered relevant since real coatings will have cracked by then and the present model is no longer applicable.

IV. RESULTS AND DISCUSSION

A. Perfect interface

For the purpose of reference, we first consider a system with a perfect interface; i.e., its strength is sufficiently higher than the stresses induced by the particular loading. This can be achieved by rigidly connecting the coating to the substrate, which corresponds to taking $\sigma_{max}/\sigma_y \to \infty$. Of particular relevance here, is the development of the stress distribution along the interface during the unloading stage and, in particular, the component normal to the interface σ_n. From this, we can already get qualitative insight into when and where delamination may occur.

Figure 3 shows the normal stress at the interface at different instants between maximum indentation depth and complete retraction of the indenter, as specified through the load F relative to the maximum indenter load. At the maximum indentation depth, the interface stress is of course compressive and almost uniform over the current contact area due to plastic flow in the substrate. The compressive stress attains a peak value of approximately 4 GPa just outside the contact region of radius a_{max}. Relatively low tensile normal stresses are found beyond the compressive region, at $r \approx 3a_{max}$. This

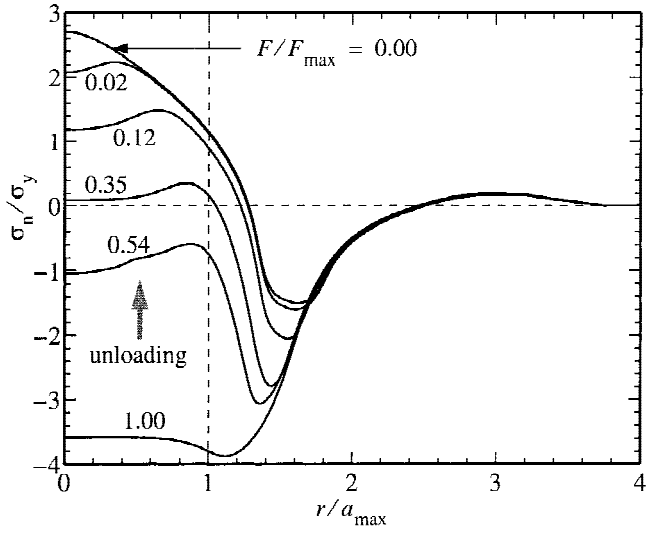

FIG. 3. Normal stress variations along a perfect interface at the beginning of unloading ($F = F_{max}$) until complete retrieval of the indenter ($F = 0$).

is a result of the resistance of the substrate to the film bending in this region. It was demonstrated by the authors[8] that the normal displacement induced by this stress will reduce the interfacial shear strength [Fig. 2(b)], which in turn may lead to shear delamination.

As the indenter is withdrawn, at the same rate as during loading, the elastically bent coating tends to seek its original flat shape. For the material parameters here this peeling tendency induces reverse plastic flow in the substrate under the indenter. As this proceeds, the initially compressive stress evolves into a tensile stress in the interface directly under the initial contact region (Fig. 3). The figure also shows that the tensile area increases slowly in size during the process of unloading, and its final size is roughly the same as the maximum contact radius a_{max}.

To study the evolution of the tensile normal stress at the interface, its maximum value σ_n^{max} is recorded together with its position r along the interface, as shown in Fig. 4. In the initial stages of unloading, tension is found only in the ring outside the contact area (Fig. 3). Upon continued unloading, the peeling effect causes interfacial tension to develop rapidly, Fig. 4(a), with the location of the maximum closely following the instantaneous contact radius a [Fig. 4(b)]. The largest value of $\sigma_n^{max} = 2.7$ GPa obtained in this particular case is reached at the end of the unloading and located at the symmetry axis.

On the basis of these results, interfacial failure leading to normal delamination may be expected during the unloading stage when the interfacial strength σ_{max} is lower than the maximum tensile stress σ_n^{max} reached at any moment. In the present case, normal delamination is avoided on the other hand if the interfacial strength σ_{max} exceeds 2.7 GPa.

Figure 5, curve (e), shows the indentation load versus displacement curve for this case of a perfect interface. Such a curve is one of the most common outputs of indentation experiments. Its importance stems from the fact that it is a signature of the indented material system. Several techniques have been reported in the literature to extract the mechanical properties of both homogeneous and composite or coated materials from indentation experiments (e.g., Refs. 13–17). In the forthcoming section, we will therefore study the interfacial failure process in more detail and provide some qualitative measures of the interfacial strength.

B. Finite-strength interface

In this section, and throughout the rest of this paper, we will study interfaces with finite strengths to allow for interfacial delamination to develop. To demonstrate the effect of the interfacial failure on the load–displacement data, Fig. 5 shows the predicted curves for different values of interfacial strength σ_{max}. The rest of the material

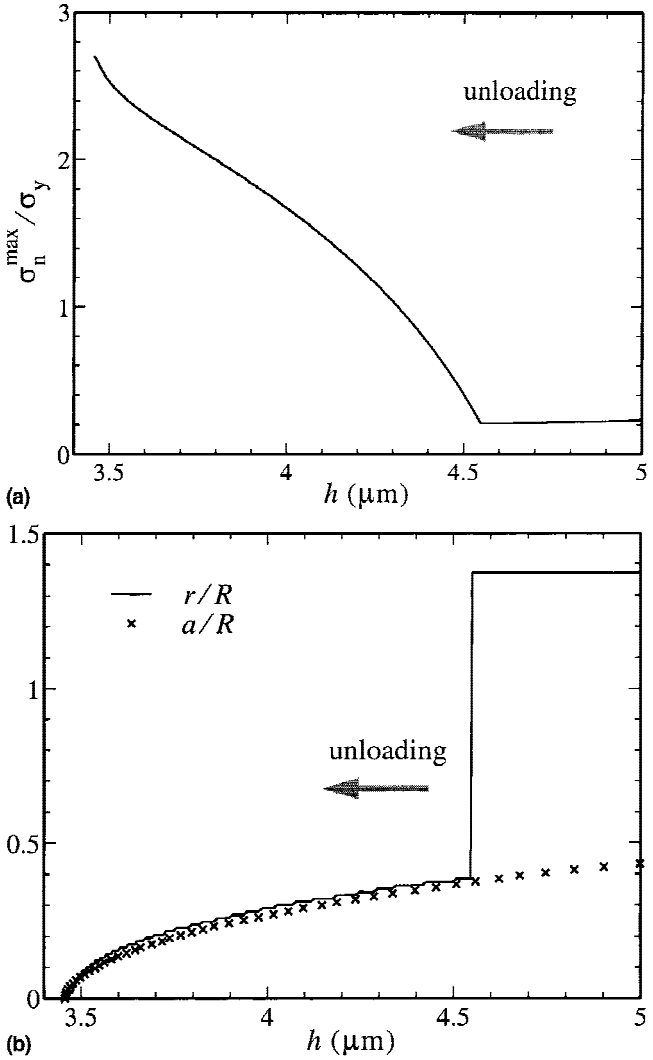

FIG. 4. (a) Evolution of the maximum normal stress σ_n^{max} with indentation depth during unloading. (b) Corresponding location at the interface at which the stress is maximum.

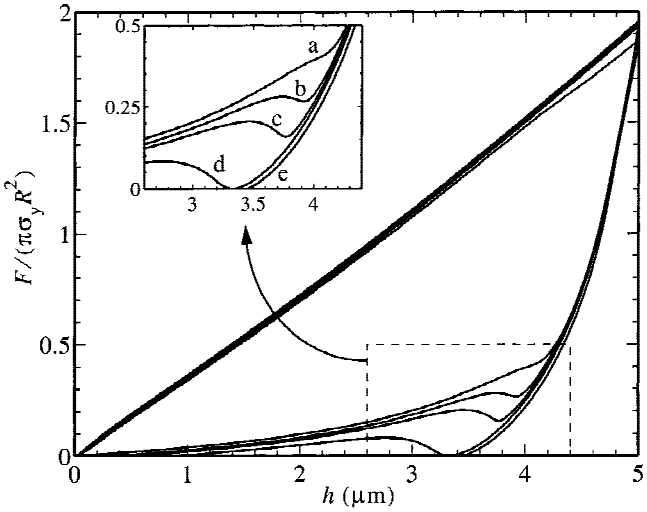

FIG. 5. Load versus displacement curves for several values of interfacial strength σ_{max}: (a) 0.55; (b) 1.1; (c) 1.5; (d) 2.2 GPa. Curve (e) is for a perfect interface.

and geometrical parameters are the same as before. Interfacial delamination during unloading was found in all cases shown in Fig. 5 (except case e). Compared to the perfect interface case (curve e), the initiation of delamination is seen to result in a rather sudden reduction of the unloading stiffness at sufficiently small F. For higher interfacial strengths, delamination is imprinted on the load versus displacement curve as a hump where the stiffness becomes negative. This phenomena will be explained in more detail later in this section. Another characteristic of delamination that can be observed in the load–displacement curve is the negligible residual indentation depth at the end of the unloading. In the absence of delamination (case e), the residual indentation depth is more than half the maximum indentation depth. Curve a, which corresponds to the lowest σ_{max}, shows a little decrease in the stiffness at the end of the loading stage. This reduction is due to shear delamination at that stage, as discussed in detail in Ref. 8. In all other cases shown, the interface strength was large enough to prevent shear delamination but not normal delamination.

The interfacial strength above which delamination is prevented is found to be $\sigma_{max} = 2.21$ GPa (curve d in Fig. 5). From the results discussed above for a perfect interface, however, we expected delamination at even higher strengths, up to 2.7 GPa. The difference must be attributed to the fact that the cohesive surface description for the finite-strength interface provides additional compliance to the system even before failure. This additional compliance results from the limited normal opening at the interface ($\Delta_n < \delta_n$), whereas a perfect interface, by definition, does not allow such opening. Although the energy consumed at the interface in this state is extremely small, the extra compliance does give rise to a small redistribution of the normal stress over the interface and a reduction of the maximum normal stress σ_n^{max}.

Figure 6(a) shows a contour plot of the von Mises effective stress at the end of the loading stage ($F = F_{max}$) for the case (c) in Fig. 5 with $\sigma_{max} = 1.5$ GPa. The size of the plastic zone at this depth of $h = 2t$ is about 5 times the maximum contact radius. To illustrate the delamination process, Fig. 6(b) shows a contour plot of the vertical stress component σ_{zz} at the end of the unloading process ($F = 0$). The first thing to observe is that the radius of the delaminated zone, r_d, is about 50% larger than the maximum contact radius a_{max} reached during indentation. Second, we observe a region with compressive normal stress in front of the delamination tip. This region is the remainder of the compressive region generated during the loading stage, which has apparently hardly changed during unloading. It thus seemed that

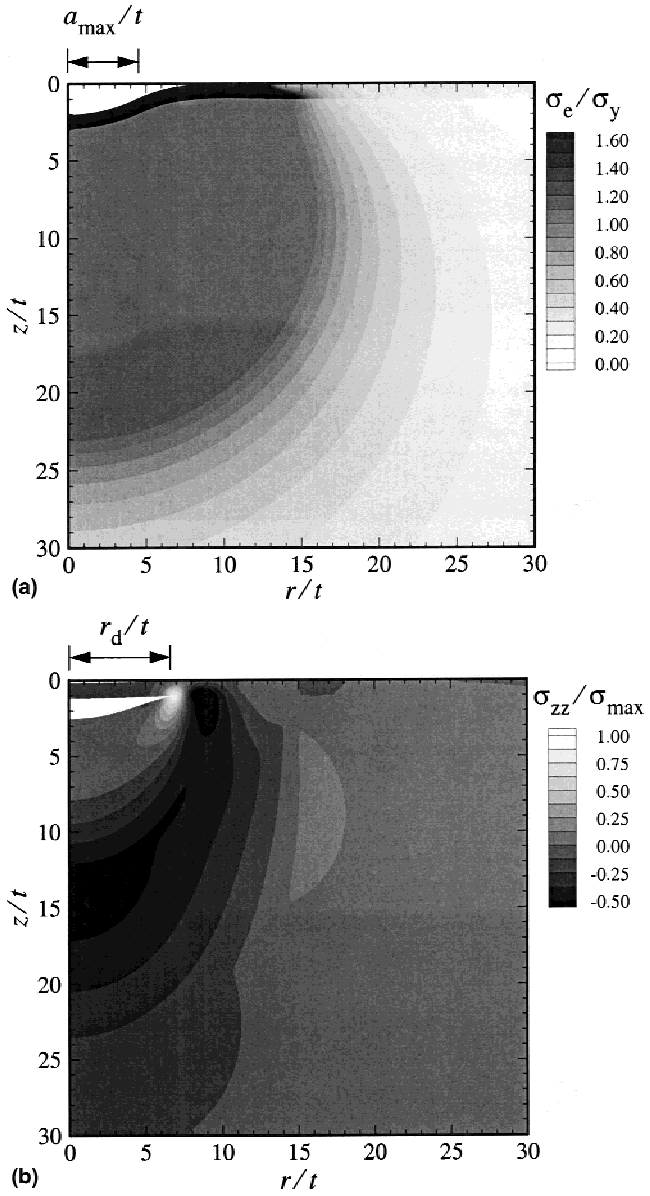

FIG. 6. (a) Contour plot of the von Mises stress at the end of loading ($F = F_{max}$). (b) Contour plot of the stress component σ_{zz} at the end of the unloading ($F = 0$) for $\sigma_{max} = 1.5$ GPa (curve c in Fig. 5). The plot also shows the delaminated region.

delamination was initiated under the retrieving indenter, expanded in the radial direction and was arrested in this compressive interfacial stress region.

The progressive development of delamination with continued unloading is shown in Fig. 7 for several values of σ_{max}. It should be noted that, except for $\sigma_{max} = 2.2$ GPa, delamination starts at a distance from the symmetry axis. For these cases r_d represents the location of the delamination tip which is traveling away from the symmetry axis. Since the other tip reaches the symmetry axis almost immediately, r_d can be considered to a good approximation as the radius of the delaminated circular area. In all cases shown in Fig. 7 delamination starts

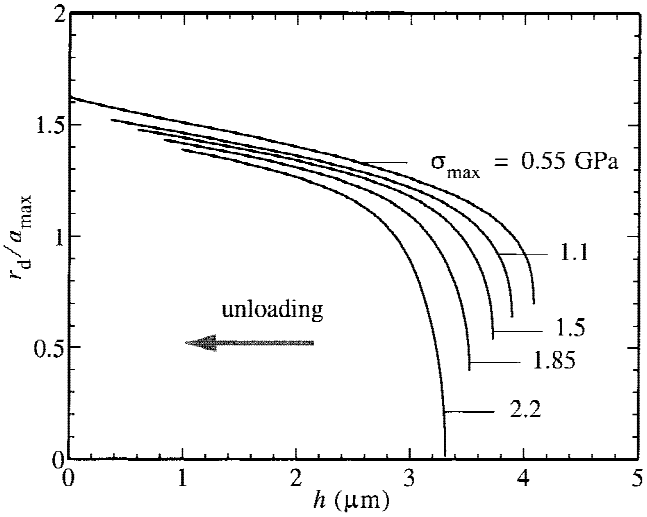

FIG. 7. Evolution of the delamination radius during unloading for $h_{max} = 5$ μm and several values of σ_{max} (or equivalently ϕ_n).

at a relatively high initial propagation velocity compared to the indentation rate $\dot{h}$ and then reaches a lower velocity on the order of $\dot{h}$. The crack is stopped when it reaches the region with sufficiently high compressive stress (Fig. 6). The final delamination radius is about 1.5 times the maximum contact area for all values of σ_{max}. It is clear in the figure that for lower interfacial strengths, delamination starts earlier in the unloading process. On the other hand, the lower the interfacial strength, the lower the residual indentation depth h_r (permanent indentation depth left at the end of the unloading). Figure 7 reveals that residual indentation depth h_r for several values of $\sigma_{max} = 0.55$ GPa. Lower interfacial strengths even lead to small negative residual indentation depths, where the coating bulges upwards at the end of the unloading.

The observations indicate that delamination is the outcome of a complex interaction between various mechanisms. To get further insight into this competition, Fig. 8(a) shows the decomposition of the total energy of the system into interfacial energy U_{in}, elastic energy U_{el} (in the film and substrate), and dissipated, plastic energy U_{pl} for the case of $\sigma_{max} = 1.5$ GPa (curve c in Fig. 5). Other values of interfacial strength show the same qualitative behavior. In this particular case, delamination initiated at $h = 1.5t = 3.75$ μm. It is clear in the figure that the plastic energy is constant at the initial stage of the unloading, i.e., the initial stage for the unloading is almost purely elastic. This is in agreement with what is commonly observed in indentation experiments Ref. 13. Limited reverse plasticity is seen to have contributed to a little increase (less than 10%) in the plastic energy. At the onset of delamination, the plastic energy reaches a constant value. The contribution of the film and the substrate to the elastic energy is demonstrated in Fig. 8(b). The

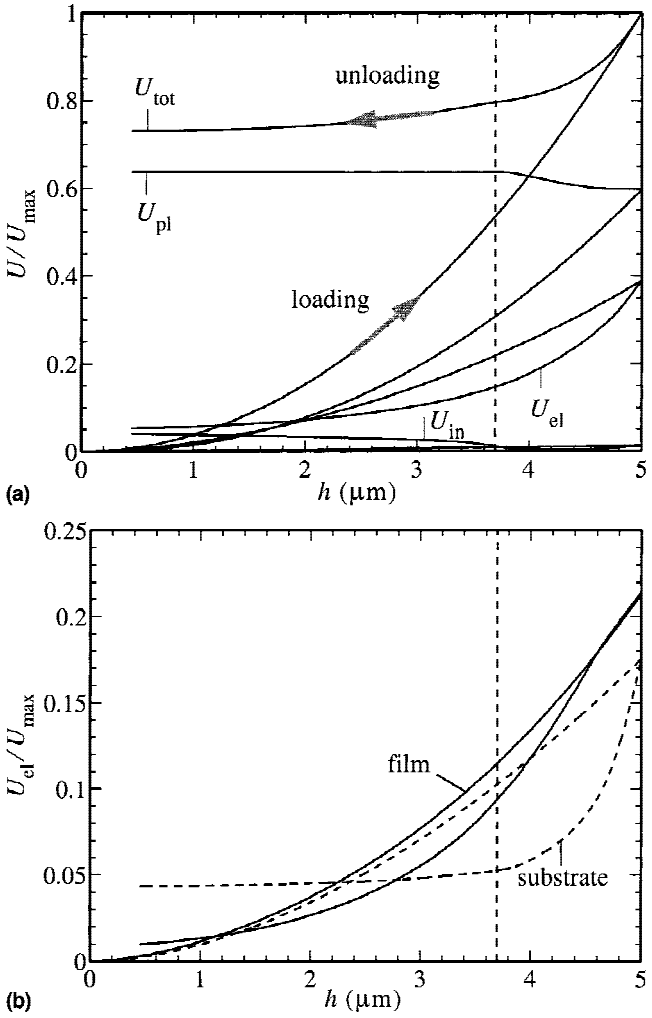

FIG. 8. (a) Decomposition of total energy into interfacial energy (U_{in}), elastic energy (U_{el}), and plastic energy (U_{pl}). (b) Contribution of the film and substrate to the elastic energy. In (a) and (b) $\sigma_{max} = 1.5$ GPa, the normalization constant is $U_{max} = \int_0^{h_{max}} F\, dh$, and the vertical dashed lines identify the initiation of delamination.

elastic energy of the substrate is seen to decrease more rapidly compared to the elastic energy of the film at the initial stage of the unloading. This is in agreement with what is reported in the literature that the initial stiffness of the unloading is predominantly controlled by the substrate for indentation depths larger than the film thickness.[13–17] At the onset of delamination, the substrate elastic energy reaches a constant value, whereas the film elastic energy decreases as the film unbends. This indicates that the main contribution to the energy release, and hence the advance of delamination, come from the film. It is also interesting to notice that, at the end of the unloading, there still exists some elastic energy in the system. This energy is small compared to the dissipated energy (plastic energy), but when compared with the interfacial energy, U_{in}, it seems to have a significant value.

On the basis of the above observations, the unstable part of the load–displacement curves, with negative stiffness, shown in Fig. 7, is now readily attributed to the spontaneous opening of the interface at the initial stage of delamination (Fig. 7). As explained in the previous paragraph and shown in Fig. 8, the processes that control the system during delamination are the unflexing of the coating and the interfacial delamination. The coating evidently provides a positive contribution to the overall stiffness, whereas the energy release from the interface gives a negative contribution. This can be seen in Fig. 8, where the stiffness provided by each energy source is the curvature of the corresponding curve. For relatively strong interfaces, the energy release from the interface dominates during the first stage of delamination when the rate of propagation, relative to the indentation rate $\dot{h}$, is high. During the second stage, the process is governed by the unflexing of the coating, thus giving rise to a positive overall stiffness (note that the coating response is constrained by the indenter which is withdrawn at a given rate). It is this complex interplay between these two terms which shapes the overall behavior of the system, including the load–displacement curve.

C. Comparison with a simple estimate

Deduction of quantitative information about the interfacial strength from indentation experiments, in particular from load–displacement curves and delamination areas, is hindered by the rather complicated interplay between the film elastic energy and the interfacial energy. A simple estimate for the work of interfacial debonding from final delamination results has been given by Hainsworth *et al.*[6] This estimate is based on an energy balance involving the interfacial energy and the elastic energy in the coating (the elastic energy in the substrate is neglected). The latter is approximated by the elastic energy of a centrally loaded disc of radius r_d with clamped edges. On the basis of this model, the interfacial work of separation is estimated by

$$\phi_n^{est} = \frac{2E_c t^3 (h_{max}^2 - h_r^2)}{3(1 - \nu_c^2) r_d^4} \quad , \qquad (13)$$

in terms of directly measurable quantities.

As the model shows a strong dependence on the coating thickness t and the maximum indentation depth h_{max}, we have chosen to vary these two parameters over a certain range and compare the model predictions with our FEM findings. A set of calculations using a conical indenter with a 68° semiangle is also performed to examine the model's sensitivity to the indenter's geometry which is not captured by Eq. (13).

Despite its very approximate nature, Eq. (13) does capture some of the qualitative trends, as shown in Fig. 9. For instance, one expects from (13) that $r_d^2 \propto h_{max}$ for a given interfacial strength (or energy) and coating properties (and neglecting the residual indentation depth).

The results of a series computations for two different strengths are summarized in Fig. 9(a) and are seen to be consistent with this scaling. The conical indenter results presented in the figure show the same trend. Sánchez *et al.*[7] have used Eq. (13) and a modified version of it on their cross-sectional indentation data, and they have also confirmed the linear relation between the delamination area and the maximum deflection of the coating. Second, according to (13), $r_d^{4/3}$ is proportional to t, with all other quantities being the same. Our results, shown in Fig. 9(b) are consistent with this as well. Finally, over the range of E_c = 350–600 GPa, the proportionality between r_d^4 and E_c is also found to be consistent with the prediction of Eq. (13).

However, not all trends are correct. For example, Eq. (13) predicts a lower slope for the delamination area versus h_{max} curve for higher values of interfacial strength, whereas the FEM results presented in Fig.9(a) show the opposite tendency.

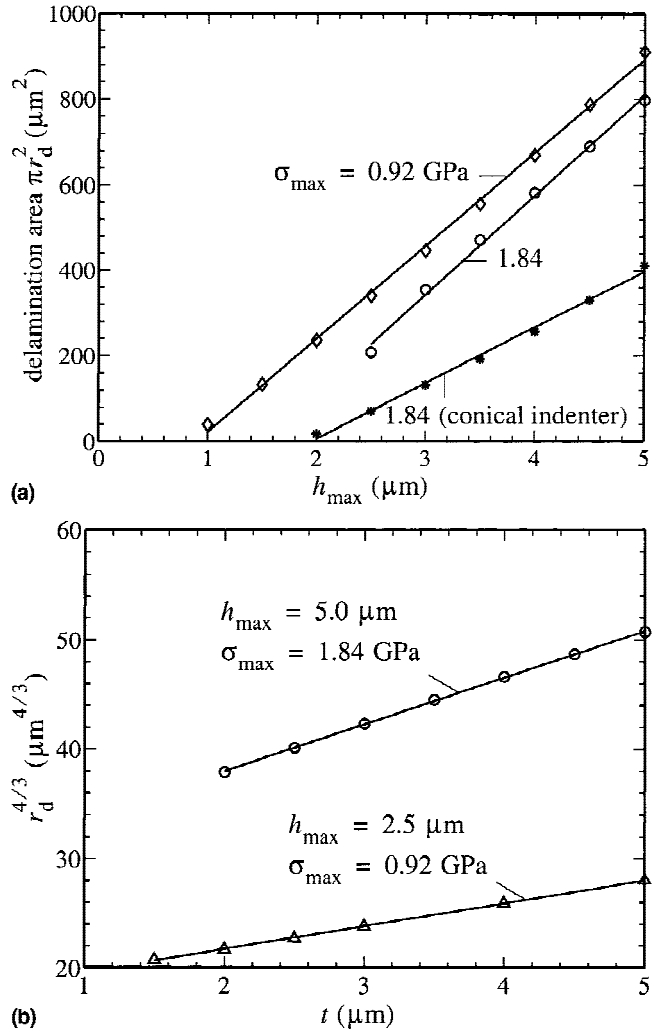

FIG. 9. (a) Delamination area πr_d^2 versus the maximum indentation depth h_{max}. (b) $r_d^{4/3}$ versus coating thickness t.

The more serious limitation of Eq. (13) is that the interfacial energy estimated from the numerical results do not agree quantitatively with the actual energies. As demonstrated in Tables I–III, the interfacial energies are severely overestimated. In Table I we notice that the higher the maximum indentation depth, the better the estimate. This can be understood by recalling that the model is based on the expression for the deflection of a clamped disc loaded at the center,[18] where the deformation is assumed to be pure bending. The contribution of the stretching is ignored; this is reasonable when the radius of the disc is large compared to its thickness. In the case of indentation, this condition is analogous to contact radius (or maximum indentation depth) being larger than the film thickness. This explains the better estimation at larger maximum indentation depths. This trend is also observed for the conical indenter in Table II, but the quality of the estimate here is even worse. The reason is that the cone produces more stretching of the film than the sphere, resulting in less accuracy of the model. In Table III, the smaller the coating thickness, the better the estimate according to Eq. (13). The same explanation

TABLE I. Estimates for ϕ_n from Eq. (13) on the basis of the computed values h_r and r_d for t = 2.5 μm and several values of h_{max}. The actual value is ϕ_n = 500 J/m^2.

h_{max} (μm)	h_r (μm)	r_d (μm)	ϕ_n^{est}/ϕ_n
2.5	0.79	8.14	15.02
3.0	0.67	10.62	7.86
3.5	0.64	12.25	6.15
4.0	0.64	13.61	5.32
4.5	0.63	14.82	4.82
5.0	0.63	15.94	4.46

TABLE II. Same as in Table I but for a conical indenter.

h_{max} (μm)	h_r (μm)	r_d (μm)	ϕ_n^{est}/ϕ_n
2.5	0.43	4.75	139.34
3.0	0.42	6.49	58.24
3.5	0.43	7.81	37.92
4.0	0.45	9.03	27.84
4.5	0.47	10.24	21.32
5.0	0.49	11.45	16.86

TABLE III. Estimates for ϕ_n from E8. (13) on the basis of the computed values of h_r and r_d for h_{max} = 5 μm and several values of t. The actual value is ϕ_n = 500 J/m^2.

t (μm)	h_r (μm)	r_d (μm)	ϕ_n^{est}/ϕ_n
2.5	0.63	15.94	4.46
3.0	0.58	16.59	6.58
3.5	0.56	17.23	9.00
4.0	0.54	17.84	11.69
4.5	0.54	18.43	14.62
5.0	0.54	19.00	17.75

holds here too. Evidently, the assumption that the disc is clamped at its boundary in questionable. If it is assumed that the disc is simply supported, the expression for ϕ_n^{est} in Eq. 13 must be multiplied by $(1 + \nu_c)/(3 + \nu_c)$. This will give better estimates, but large errors are still possible.

Note that Eq. 13 does not incorporate the influence of the substrate. To see the accuracy of this approximation, we have investigated the dependence of the delamination radius r_d on the substrate properties E_s and σ_y. Varying the substrate Young's modulus E_s from 100 to 500 GPa, the resulting delamination radius increases with E_s by 25%. On the other hand, an increase of the yield stress σ_y from 0.72 to 2.0 GPa gives values of r_d that decrease by only 6%. The reason for this is that the yield stress determines the size of the plastic zone in the substrate but not the permanent deformation immediately below the indenter; the latter is what is controlling the delamination radius. However, it should be noted, as will be discussed in the next section, that the yield stress plays a major role in determining whether delamination will take place at all.

D. Critical value of interfacial strength for delamination

Whether or not delamination takes place depends on the tensile normal stress that can be generated at the interface during the unloading process. The ultimate value of this stress relative to the interface strength σ_{max} depends on almost all parameters involved in the boundary value problem in a rather complex way. We have performed a parameter study involving the coating elastic modulus, the substrate yield stress, the maximum indentation depth, and the coating thickness. For each parameter combination, delamination is suppressed if the interfacial strength is higher than a critical value of σ_{max}^c.

As an example, Fig. 10 shows load–displacement curves for different values of maximum indentation depths. Delamination is seen to occur if h_{max} is above a certain critical value, and it is recognized by the hump left on the curve and the negligible residual indentation depth. Lower indentation depths do not create normal stresses that exceed the interfacial strength σ_{max} and, therefore, do not lead to delamination.

Figure 11 shows the variation of the critical strength σ_{max}^c with (a) the maximum indentation depth, (b) the coating thickness, (c) the coating Young's modulus, and (d) the substrate yield stress. Higher values of the coating Young's modulus E_c, the coating thickness t^3, or the maximum indentation depth h_{max} lead to delamination of stronger interfaces. These are explained by the fact that the driving force for delamination is the unbending of the coating. Despite the limitations of the circular disc model pointed out before, these trends are roughly consistent with Eq. (13) but not when looked at in more detail.

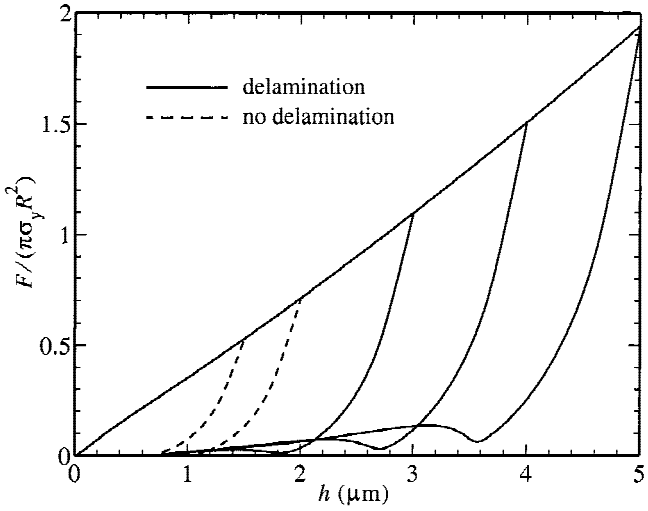

FIG. 10. Load–displacement curves for several values of h_{max}, for a coating strength of $\sigma_{max} = 1.85$ GPa.

For values of h_{max} less than the coating thickness ($t = 2.5$ μm), σ_{max}^c shows a relatively rapid increase, Fig. 11(a). This increase is attributed to the increase in the bending moment in the coating. The bending moment is proportional to the curvature of the coating which increases rapidly with the indentation depth until the coating takes the shape of the indenter. After that point, the curvature does not change much but the bent region propagates outward, and this corresponds to the slower increase in σ_{max}^c for higher indentation depths. Figure 11(b) shows also an initial rapid increase in the critical strength with the coating thickness due to the increase of the bending moment with t^3. For thicker coatings, the critical strength decreases due to the decrease in the coating curvature because the substrate becomes relatively softer. Figure 11(c) shows an almost linear increase of the critical strength with the coating Young's modulus. The increase of the critical strength with the substrate yield stress σ_y is shown in Fig. 11(d). This increase is caused by the reverse plasticity that takes place prior to delamination (Fig. 8). The higher the yield stress, the higher the stresses which can be reached at the substrate. Since the normal stress is continuous across the interface, higher tensile normal stress can be reached with increasing σ_y, thus making it possible to delaminate stronger interfaces.

E. Residual stresses and interfacial waviness

Coated systems generally contain residual stresses. These are due to the deposition process itself, to the thermal expansion mismatch between the coating and the substrate, or a combination of the two. To study the influence of residual stresses on delamination, we have introduced uniform in-plane stress in the film prior to indentation. This has been achieved, for numerical

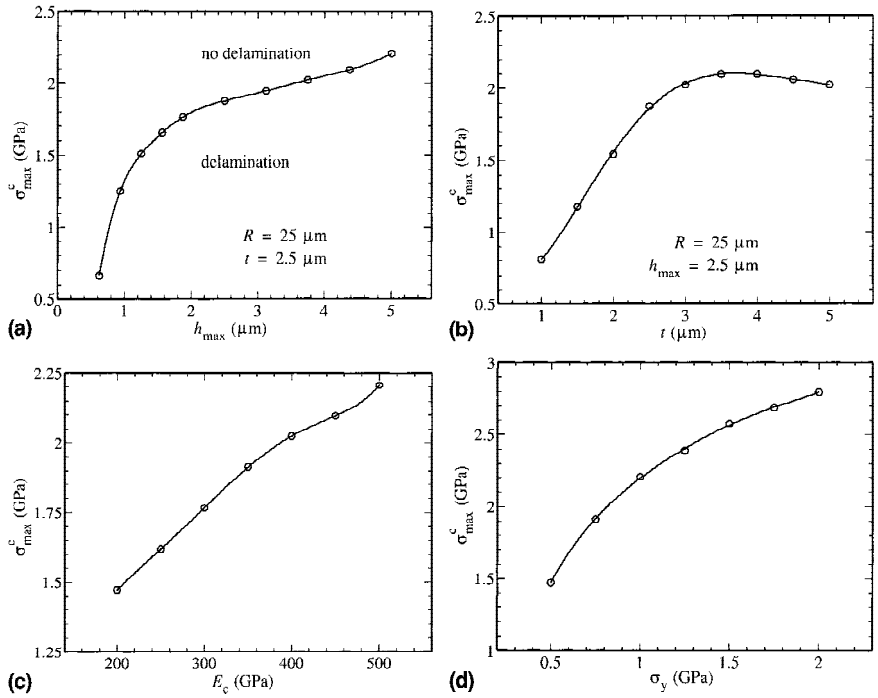

FIG. 11. Critical value of the interfacial strength σ^c_{max} versus (a) h_{max}, (b) t, (c) E_c, and (d) σ_y.

convenience, by assigning different thermal expansion coefficients to coating and substrate and by subjecting the system to various temperature changes to generate stresses ranging from −10 GPa (compressive) to 10 GPa (tensile). Subsequently, we perform the indentation calculations as before.

Compressive stress in the coating is found to delay the delamination process, or to even prevent delamination, whereas the opposite happens with tensile stresses. This is explained by the fact that residual stress will have an out-of-plane component after the deformation of the coating. In the case of tensile stress, this component will tend to enhance the unbending of coating during the unloading and, thus, will assist delamination. As a consequence, the critical strength to prevent delamination will increase with residual tension in the coating. Compressive stress has the opposite effect. For example, a coating of the default thickness of $t = 2.5$ μm with a interfacial strength of $\sigma_{max} = 1.84$ GPa was found earlier to delaminate after indentation to $h_{max} = 5$ μm [see Fig. 11(a)], but delamination is prevented under a residual stress of −10 GPa. The delamination radius r_d is relatively insensitive to the residual stress: over a range of −7.5 to 10 GPa, r_d varies between 14.4 and 16.7 μm compared to $r_d = 15.94$ μm for the stress-free coating (cf. Table I).

Roughness of the interface is commonly simplified by a sinusoidal wave (e.g., Ref. 19). To study the effect of roughness on delamination, a wave of an amplitude up to $0.2t$ and a wavelength up to $2t$ were introduced along the interface; see Fig. 12. Delamination is found to start at valleys and crests where the normal stress component has a local maximum. Neighboring delaminated areas link up before the delamination front propagates to the next crest/valley. Even though the precise evolution of delamination depends on the waviness of the interface, for

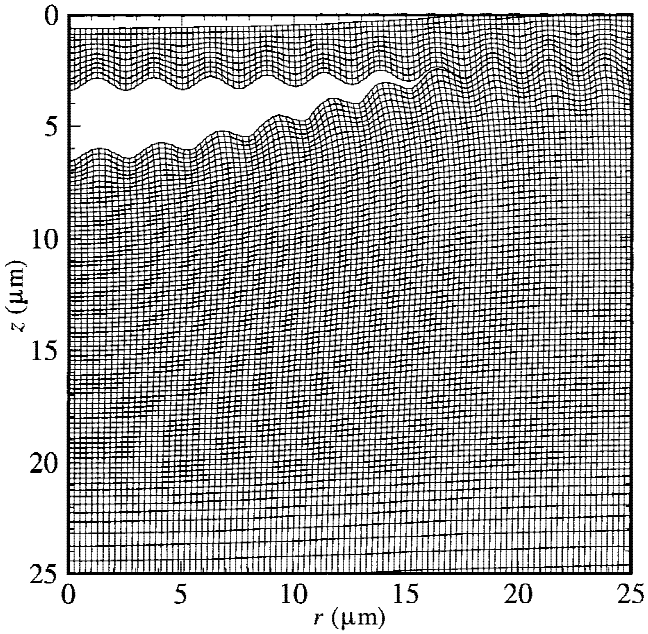

FIG. 12. Example of normal delamination for a case with a rough interface, modeled as a sinusoidal wave with an amplitude of $0.12t$ and a wavelength equal to t. In this case, $h_{max} = 5$ μm and $\sigma_{max} = 1.85$ GPa.

all cases considered here we did not find a significant effect on the critical indentation depth at which delamination starts nor on the final delamination radius.

V. CONCLUSIONS

For the purpose of studying interfacial delamination, numerical simulations have been carried out of the indentation process of a coated material by a spherical indenter. To describe interfacial failure, the interface between the film and the substrate was modeled by means of a cohesive surface, with a coupled constitutive law for the normal and the tangential response. Failure of the interface by normal or tangential separation, or a combination, is embedded in the constitutive model and does not require any additional criteria.

Normal delamination occurs during the unloading stage of the indentation process. A circular part of the coating, directly under the contact area, is lifted off from the substrate, driven by the bending moment in the coating. Normal delamination is recognized by the imprint left on the load versus displacement curve and the negligible residual indentation depth. For any given indentation depth, the normal stress that can be attained at the interface is larger for thicker coatings, for coatings with a higher Young's modulus, or for substrates with a higher yield strength. To prevent delamination of such coatings, stronger interfaces are necessary.

It should be noted that shear delamination can occur during indentation, before normal delamination takes place. Compared to normal delamination, shear delamination can occur for relatively low interfacial strength. Conversely, if the interface strength is high enough to prevent normal delamination, shear delamination will also be avoided.

The energy consumed by the delamination process has been explicitly calculated and separated from the part dissipated by plastic deformation in the substrate. A small amount of elastic energy, but still comparable with the total interfacial energy, is left in the system after unloading. Delamination is driven by the coating energy as it unflexes to retain its initial configuration. Deduction of quantitative information about the interfacial work of separation or strength is hindered by the complex interplay between the coating elastic energy and the interfacial energy. However, the present model does allow for an inverse approach by which the work of separation can be derived iteratively.

The disc model estimate[6] has been compared with our numerical findings for a range of parameters. It does capture some of the qualitative aspects of delamination. But, it tends to strongly overestimate the interfacial strength or energy of separation.

Critical values of the interfacial strength were calculated for several parameter combinations. The general trends of the variation of these critical values with the involved parameters are easily interpreted, whereas the details of this variation are governed by the nonlinear nature of the problem.

Compressive residual stress in the film delays delamination, and if high enough, it might even prevent delamination, whereas tensile residual stress has an opposite effect. Waviness of the interface was not found to have a significant effect on delamination. Both conclusions, however, are intimately tied to the assumption that the coating remains intact during indentation.

REFERENCES

1. M.D. Kriese and W.W. Gerberich, J. Mater. Res. **14,** 3019 (1999).
2. X. Li and B. Bhushan, Thin Solid Films **315,** 214 (1998).
3. A. Bagchi and A.G. Evans, Interface Sci. **3,** 169 (1996).
4. B.D. Marshall and A.G. Evans, J. Appl. Phys. **56,** 2632 (1984).
5. M.D. Drory and J.W. Hutchinson, Proc. R. Soc. London, Ser. A **452,** 2319 (1996).
6. S.V. Hainsworth, M.R. McGurk, and T.F. Page, Surf. Coat. Technol. **102,** 97 (1998).
7. J.M. Sánchez, S. El-Mansy, B. Sun, T. Scherban, N. Fang, D. Pantsuo, W. Ford, M.R. Elizalde, J.M. Martínez-Esnaola, A. Martín-Meizoso, J. Gil-Sevillano, M. Fuentes, and J. Maiz, Acta Mater. **47,** 4405 (1999).
8. A. Abdul-Baqi and E. Van der Giessen, Thin Solid Films **381,** 143 (2001).
9. X-P. Xu and A. Needleman, Model. Simul. Mater. Sci. Eng. **1,** 111 (1993).
10. R. Becker, A. Needleman, O. Richmond, and V. Tvergaard, J. Mech. Phys. Solids **36,** 317 (1988).
11. Y. Wei and J.W. Hutchinson, Int. J. Fract. **10,** (1999).
12. X-P. Xu and A. Needleman, J. Mech. Phys. Solids **42,** 1397 (1994).
13. M. Doerner and W. Nix, J. Mater. Res. **4,** 601 (1986).
14. A.K. Bhattacharya and W.D. Nix, Int. J. Solids Struct. **24,** 1287 (1988).
15. H. Gao, C-H. Chiu, and J. Lee, Int. J. Solids Struct. **29,** 2471 (1992).
16. R.B. King, Int. J. Solids Struct. **23,** 1657 (1987).
17. Y.Y. Lim, M.M. Chaudhri, and Y. Enomoto, J. Mater. Res. **14,** 2314 (1999).
18. S. Timoshinko and S. Woinowsky-Krieger, *Theory of Plates and Shells,* 2nd ed. (McGraw-Hill, New York, 1959).
19. D.R. Clarke and W. Pompe, Acta Mater. **47,** 1749 (1999).